This space is reserved for the EPiC Series header, do not use it

Reachability Analysis of Transformer-Isolated DC-DC Converters (Benchmark Proposal)

Omar A. Beg[1], Ali Davoudi[1], and Taylor T. Johnson[2]

[1] University of Texas at Arlington, Arlington, Texas, USA
omar.beg@mavs.uta.edu, davoudi@uta.edu
[2] Vanderbilt University, Nashville, Tennessee, USA
taylor.johnson@vanderbilt.edu

Abstract

Various mission-critical applications necessarily require a transformer in switching converters to obtain DC isolation between the converters' input and output. Since DC-DC converters are the switching devices, these are molded as hybrid automata. We present hybrid automaton modeling of two main types of transformer isolated DC-DC converters, namely, flyback and forward converters. We use HyST (Hybrid Source Transformation) tool to automatically generate the models in SpaceEx format, perform reachability analysis, and then automatically convert the models into Mathworks Simulink Stateflow (SLSF) using HyST. Thus we demonstrate effectiveness of HyST tool in the model-based design process. The HyST user needs not to manually construct or modify the models thus saving significant amount of time and efforts.

Category: academic **Difficulty:** medium

1 Context and Origins

DC-DC convertrs are the power electronics devices that are extensively used in automotives, industrial, and defense related applications and their mission-critical nature necessitates formal verification prior implementation. Over the period, there has been a drastic rise in power electronics-related safety recalls in the automotive industry. For example, the main cause for recall of around 700,000 Toyota Prius cars in 2014 was attributed to an error in the interaction between a boost converter and its software controller [7]. Likewise, more than 100,000 Toyota Prius cars were recalled due to an inverter failure [8]. Therefore, this mission-critical domain would require significant confidence in the modeling accuracy. This can be ensured through reachability analysis [1]. We present two potential benchmarks related to transformer-isolated DC-DC converters for hybrid verification research community. Transformer isolation is implemendted by introducing a transformer at the converter input. In addition to the electrical isolation between the input and the output, transformer-isolated DC-DC converters have some advantages compared to the non-isolated converters such as high efficiency and low manufacturing cost [3]. This work is based on hybrid automaton modeling of two main types of

transformer-isolated DC-DC converters, i.e., flyback converter and forward converter. This is a series of benchmarks that are being developed to benefit from formal verification prior to field implementation and deployment.

Flyback converter may be regarded as a transformer-isolated buck-boost converter, whereas, forward converter acts as a transformer-isolated buck converter. We develop hybrid automaton models of flyback and forward converters, and use SpaceEx [4], a reachability analysis tool, to compute the over-approximated sets of reachable states [1]. This is a classical fixed point computation tool that operates on symbolic states.

We also use HyST (Hybrid Source Transformation) [2] to automatically convert the hybrid automaton models developed in SpaceEx to MathWorks Simulink/Stateflow (SLSF) models [2]. It is a source-to-source translation tool that takes input in the SpaceEx model format, and translates it to the formats of HyCreate,Flow*, dReach, C2E2, Passel 2.0, and HyComp. In addition, it is also used to automatically generate the hybrid automaton models in SpaceEx format as per user-defined parameters and settings. Additional tool support is being added from time to time. Verification and validation research community may use HyST to automatically transform the hybrid automaton models in SpaceEx format to other formats and perform reachability analysis using aforesaid model checking tools.

2 Hybrid Automaton Modeling of Transformer-Isolated DC-DC Converters

We present the hybrid automaton modeling of flyback and forward converters in this section. We assume that transformer losses are negligible with perfect coupling among the windings. The transformer is modeled using a parallel magnetizing inductance L_m at the input side, called the primary side. The winding towards the output is called the secondary winding. Let n be the turns ratio of primary to secondary windings. Let v_1 and v_2 be the voltage across primary and secondary windings, i_1 and i_2 be the respective currents, and let n_1 and n_2 be the respective number of turns. Following relation holds for an ideal transformer

$$\frac{v_1}{n_1} = \frac{v_2}{n_2}, \tag{2.1}$$

and

$$n_1 i_1 = -n_2 i_2. \tag{2.2}$$

2.1 Flyback Converter Modeling

We consider the flyback converter in open-loop configuration as shown in Figure 2.1 exported from PLECS software [5], a power electronics circuit simulator. The switching is realized by the MOSFET switch and the diode D_1. The state variables are defined by the voltage across the capacitor v_C, and current through the magnetizing inductor inductor i_{Lm}. The MOSFET switch is operated by a pulse generator of constant duty cycle D, over the switching time period T. The operation of this circuit is dependent upon the state of the MOSFET switch, i.e., being ON and OFF, resulting into two modes:

[1] The tool is available online from the SpaceEx website at: http://spaceex.imag.fr/.

[2] The executable models are included on the ARCH website and are also available online from the HyST website at: http://verivital.com/hyst/.

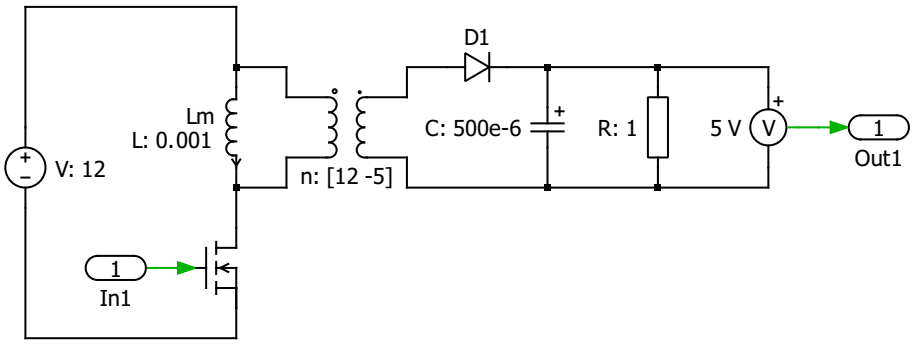

Figure 2.1: Schematic diagram of the flyback converter.

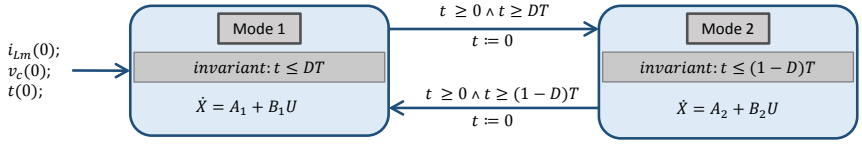

Figure 2.2: Hybrid automaton model for flyback converter.

1. Mode 1: In this mode, the MOSFET switch is ON during the switching cycle $0 < t \leq DT$, wherein, the input DC voltage V_{in} is connected to the primary of the transformer. This induces the current in the secondary winding in opposite polarity to reverse bias the diode (setting it to OFF state). In this mode, the primary of the transformer is charged, wheres, the diode acts as an open switch causing the capacitor to discharge through the load resistance. We model the MOSFET switching loss by a series resistor r_{sw}. The ordinary differential equations (ODEs) for i_{Lm} and v_C for this mode are formed using conventional Kirchoff' voltage law (KVL) and Kirchoff's current law (KCL). Applying KVL on the left loop gives

$$\frac{di_{Lm}}{dt} = \frac{r_{sw}}{L_m} i_{Lm} + \frac{V_{in}}{L_m}, \tag{2.3}$$

whereas, applying KVL on the loop containing R and C gives

$$\frac{dv_C}{dt} = \frac{1}{RC} v_C. \tag{2.4}$$

The state space matrices, during the switching cycle $0 < t \leq DT$, are thus given by

$$A_1 = \begin{bmatrix} \frac{r_{sw}}{L_m} & 0 \\ 0 & \frac{1}{RC} \end{bmatrix}, B_1 = \begin{bmatrix} \frac{1}{L_m} \\ 0 \end{bmatrix}, X = \begin{bmatrix} i_{Lm} \\ v_C \end{bmatrix}, U = \begin{bmatrix} V_{in} \\ 0 \end{bmatrix}, \tag{2.5}$$

2. Mode 2: In this mode, the MOSFET switch is OFF during the switching cycle $DT < t \leq T$, thus the input DC power supply is disconnected from the primary of the transformer. The current in the secondary flows in upward direction hence diode is forward biased (in ON state). We first consider the primary winding loop and apply KVL. Using Equation 2.1,

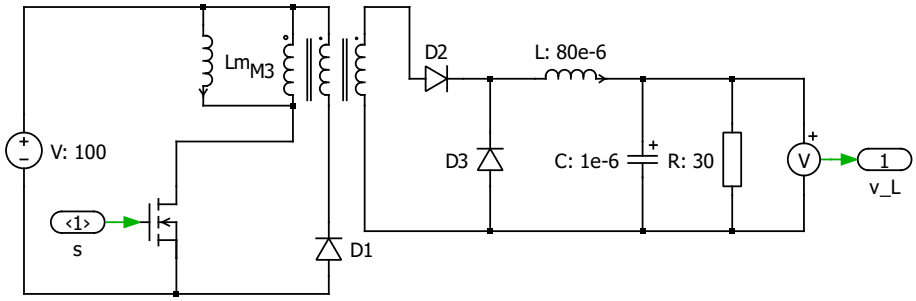

Figure 2.3: Scehmatic diagram of forward converter.

the voltage across the primary is given by

$$v_1 = -nv_C, \tag{2.6}$$

such that the negative sign is due to its opposite direction. Applying KVL in the primary winding loop, we obtain following relation for the magnetizing inductor current

$$\frac{di_{Lm}}{dt} = -\frac{n}{L_m}v_C. \tag{2.7}$$

The current through primary winding is the same as current through L_m. From Equation 2.2, the current through the secondary winding is given by

$$i_2 = ni_{Lm}. \tag{2.8}$$

Consider the node joining R and C. The current entering this node is i_2. Applying KCL on this node, we get

$$\frac{dv_C}{dt} = \frac{n}{C}i_{Lm} - \frac{1}{RC}v_C. \tag{2.9}$$

The corresponding state space matrices, during the switching cycle $DT < t \leq T$, are thus given by

$$A_1 = \begin{bmatrix} 0 & -\frac{n}{L_m} \\ \frac{n}{C} & -\frac{1}{RC} \end{bmatrix}, B_1 = \begin{bmatrix} 0 \\ 0 \end{bmatrix}. \tag{2.10}$$

We have formulated a hybrid automaton model of flyback converter using the above ODEs as shown in Figure 2.2. The component values used in the model are mentioned in Figure 2.1, and adopted from [5].

2.2 Forward Converter Modeling

The forward converter may be regarded as a transformer-isolated buck converter, as illustrated in Figure 2.3 sketched using PLECS [5]. It has a MOSFET switch, and three diodes D_1, D_2, and D_3 to realize the switching operation. We consider three state variables, i.e, magnetizing current i_{Lm}, inductor current i_L, and capacitor voltage v_C. Let n_1, n_2, and n_3 be the number of turns in three windings of the transformer. The switching modes depend on the state of the MOSFET switch as well as the fact that whether inductor current $i_L \leq 0$ and the magnetizing current $i_{Lm} \leq 0$. This results in five different modes as under.

1. Mode 1: In this mode, the MOSFET switch is ON during the switching cycle $0 < t \leq DT$, wherein, the input DC voltage V_{in} is connected to the primary winding of the transformer. This causes D_2 to become forward biased (ON), and D_1 and D_3 to become reverse biased (OFF). Applying KVL to left most loop results in

$$\frac{di_{Lm}}{dt} = \frac{V_{in}}{L_m}, \tag{2.11}$$

whereas, the voltage across D_3 is $\frac{n_3}{n_1}V_{in}$. Applying KVL to the loop containing L and C, results

$$\frac{di_L}{dt} = \frac{n_3 L}{n_1}V_{in} - \frac{1}{L}v_C. \tag{2.12}$$

Consider the node common to L, C, and R. Applying KCL here results

$$\frac{dv_C}{dt} = \frac{1}{C}i_L - \frac{1}{RC}v_C. \tag{2.13}$$

The corresponding state space matrices, during the switching cycle $0 < t \leq DT$, are thus given by

$$A_1 = \begin{bmatrix} 0 & 0 & 0 \\ 0 & 0 & -\frac{1}{L} \\ 0 & \frac{1}{C} & -\frac{1}{RC} \end{bmatrix}, B_1 = \begin{bmatrix} \frac{1}{L_m} \\ \frac{n_3}{n_1 L} \\ 0 \end{bmatrix}, X = \begin{bmatrix} i_{Lm} \\ i_L \\ v_C \end{bmatrix}, U = \begin{bmatrix} V_{in} \\ V_{in} \\ 0 \end{bmatrix}. \tag{2.14}$$

2. Mode 2: The MOSFET switch is OFF during the switching cycle $DT < t \leq (1-D)T$ such that V_{in} is disconnected from the primary winding, and both $i_{Lm} > 0$ and $i_L > 0$. The diodes D_1 and D_3 are ON, whereas, D_2 is OFF. The input voltage is applied to the winding 2 of the transformer such that the voltage across L_m is $-Vin\frac{n_1}{n_2}$. This results in decrease of i_{Lm} such that

$$\frac{di_{Lm}}{dt} = -\frac{n_1 V_{in}}{n_2 L_m}, \tag{2.15}$$

Since L discharges through the load resistor, D_3 remains ON, such that V_{in} is not available to charge the inductor L. This gives us

$$\frac{di_L}{dt} = -\frac{1}{L}v_C, \ \frac{dv_C}{dt} = \frac{1}{C}i_L - \frac{1}{RC}v_C. \tag{2.16}$$

The corresponding state space matrices are

$$A_2 = \begin{bmatrix} 0 & 0 & 0 \\ 0 & 0 & -\frac{1}{L} \\ 0 & \frac{1}{C} & -\frac{1}{RC} \end{bmatrix}, B_2 = \begin{bmatrix} -\frac{n_1}{n_2 L_m} \\ 0 \\ 0 \end{bmatrix}. \tag{2.17}$$

3. Mode 3: The MOSFET switch is still OFF during the switching cycle $DT < t \leq (1-D)T$ such that $i_{Lm} \leq 0$ and $i_L > 0$. As $i_{Lm} \leq 0$, diode D_1 becomes OFF. Overall, the MOSFET switch and diodes D_1 and D_2 are OFF. We can form another set of ODEs as

$$\frac{di_{Lm}}{dt} = 0, \ \frac{di_L}{dt} = -\frac{1}{L}v_C, \ \frac{dv_C}{dt} = \frac{1}{C}i_L - \frac{1}{RC}v_C. \tag{2.18}$$

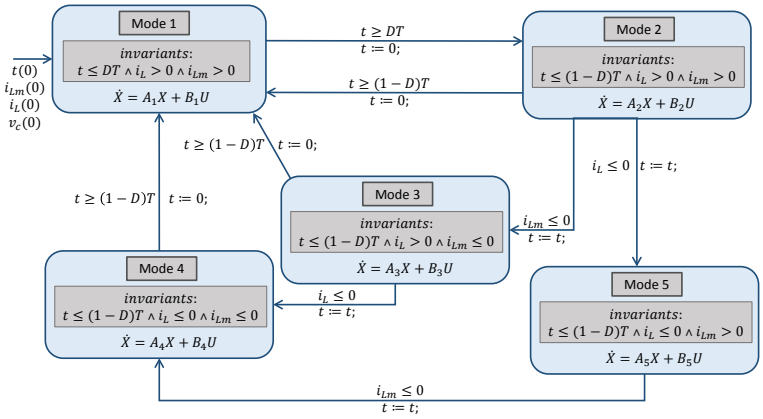

Figure 2.4: Hybrid automaton model for forward converter.

The corresponding state space matrices are

$$A_3 = \begin{bmatrix} 0 & 0 & 0 \\ 0 & 0 & -\frac{1}{L} \\ 0 & \frac{1}{C} & -\frac{1}{RC} \end{bmatrix}, B_3 = \begin{bmatrix} 0 \\ 0 \\ 0 \end{bmatrix}. \tag{2.19}$$

4. Mode 4: The MOSFET switch is OFF during the switching cycle $DT < t \le (1-D)T$ such that both and $i_{Lm} \le 0$ and $i_L \le 0$. Following set of ODEs can be formed

$$\frac{di_{Lm}}{dt} = 0, \ \frac{di_L}{dt} = 0, \ \frac{dv_C}{dt} = -\frac{1}{RC}v_C. \tag{2.20}$$

The corresponding state space matrices are

$$A_4 = \begin{bmatrix} 0 & 0 & 0 \\ 0 & 0 & -\frac{1}{L} \\ 0 & 0 & -\frac{1}{RC} \end{bmatrix}, B_4 = \begin{bmatrix} 0 \\ 0 \\ 0 \end{bmatrix}. \tag{2.21}$$

5. Mode 5: The MOSFET switch is OFF during the switching cycle $DT < t \le (1-D)T$. There is another possibility that i_L approaches zero while i_{Lm} is still non-zero, thus we have another condition $i_{Lm} > 0$ and $i_L \le 0$. This gives us

$$\frac{di_{Lm}}{dt} = -\frac{n_1V_{in}}{n_2L_m}, \ \frac{di_L}{dt} = 0, \ \frac{dv_C}{dt} = -\frac{1}{RC}v_C. \tag{2.22}$$

The corresponding state space matrices are

$$A_5 = \begin{bmatrix} 0 & 0 & 0 \\ 0 & 0 & 0 \\ 0 & 0 & -\frac{1}{RC} \end{bmatrix}, B_5 = \begin{bmatrix} -\frac{n_1}{n_2L_m} \\ 0 \\ 0 \end{bmatrix}. \tag{2.23}$$

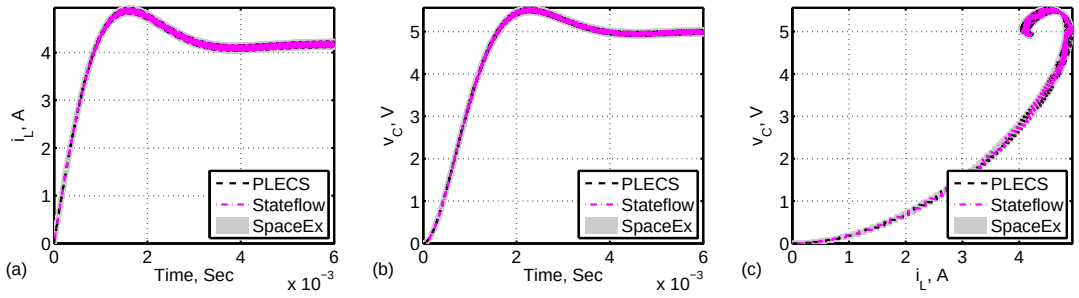

Figure 3.1: Comparison of SpaceEx reach sets, PLECS and SLSF trajectories for the flyback converter showing the simulation trace containment within overapproximated sets of reachable states: (a) Inductor current vs time (b) Capacitor voltage vs time (c) Phase-plane plot of capacitor voltage and inductor current.

Using the above ODEs, the hybrid automaton model of forward converter is formulated and shown in Figure 2.4. The component values used in the model are mentioned in Figure 2.3 and adopted from [6].

3 SLSF Simulations and Reachability Analysis

We have automatically generated the hybrid automaton models in SpaceEx format using HyST tool and analyze these in SpaceEx environment. Moreover, we have automatically translated the same SpaceEx models into SLSF format using HyST. Formal verification of the flyback converter includes verifying its capacitor voltage to attain a stable value in settling time, i.e., whether v_C attains a stable value v_{ref} within settling time s_t. SpaceEx, PLECS, SLSF results for the capacitor voltage and inductor current are shown in Figure 3.1. It is evident from the results in Figure 3.1 that PLECS and SLSF simulation traces are contained within the over-approximated sets of reachable states. We also conclude that these results exhibit stable limit cycle, and that stable voltage is attained within 5 $mSec$.

We perform the reachability analysis using SpaceEx for forward converter as shown in Figure 3.2. The SLSF time traces for the output voltage are contained within the over-approximated sets of reachable states computed using SpaceEx.

4 Key Observations

Hybrid automaton modeling and reachability analysis of transformer-isolated DC-DC converters has medium difficulty level. We have only used SpaceEx to perform the reachability analysis. In addition other reachability analysis tools may also be used for the reachability analysis.

We have not considered the parasitics in modeling of transformer-isolated DC-DC converters that will further increase the difficulty level of this benchmark.

5 Benchmark Outlook

On the whole, these verification benchmarks can serve as a first step towards a benchmark library to evaluate reachability and verification methods for various types of DC-DC converters.

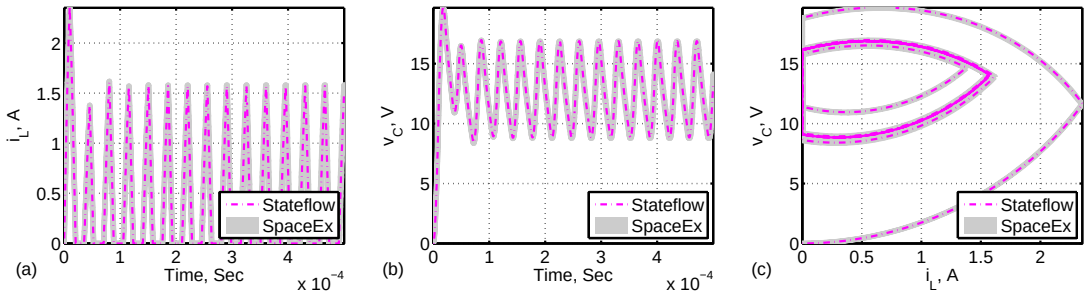

Figure 3.2: Comparison of SpaceEx and SLSF for the output voltage of forward converter, showing the simulation trace containment within overapproximated sets of reachable states: (a) Inductor current vs time (b) Capacitor voltage vs time (c) Phase-plane plot of capacitor voltage and inductor current.

These benchmarks are open to the continuous and hybrid systems verification community to evaluate their methods and tools.

Acknowledgments The material presented in this paper is based upon work supported by the National Science Foundation (NSF) under grant numbers CNS 1464311 and CCF 1527398, the Air Force Research Laboratory (AFRL) through contract number FA8750-15-1-0105, and the Air Force Office of Scientific Research (AFOSR) under contract number FA9550-15-1-0258. The U.S. government is authorized to reproduce and distribute reprints for Governmental purposes notwithstanding any copyright notation thereon. Any opinions, findings, and conclusions or recommendations expressed in this publication are those of the authors and do not necessarily reflect the views of AFRL, AFOSR, or NSF.

References

[1] Matthias Althoff, Akshay Rajhans, Bruce H. Krogh, Soner Yaldiz, Xin Li, and Larry Pileggi. Formal verification of phase-locked loops using reachability analysis and continuization. *Commun. ACM*, 56(10):97–104, October 2013.

[2] Stanley Bak, Sergiy Bogomolov, and Taylor T Johnson. Hyst: a source transformation and translation tool for hybrid automaton models. In *Proceedings of the 18th International Conference on Hybrid Systems: Computation and Control*, pages 128–133. ACM, 2015.

[3] Dae-Kyu Choi et al. A novel power conversion circuit for cost-effective battery-fuel cell hybrid systems. *Journal of Power Sources*, 152:245 – 255, 2005.

[4] Goran Frehse et al. Spaceex: Scalable verification of hybrid systems. In Shaz Qadeer Ganesh Gopalakrishnan, editor, *Proc. 23rd International Conference on Computer Aided Verification (CAV)*, LNCS. Springer, 2011.

[5] Plexim Inc., Cambridge, MA, USA. *PLECS Manual Version 4.0.4*, 2016.

[6] A. Taut et al. Educational matlab tool for simulating of forward converters. In *Proceedings of International Spring Seminar on Electronics Technology*, pages 641–644, May 2011.

[7] Toyota. Defect information report (nhtsa recall 14v-053), Feb. 12 2014.

[8] Toyota. Defect information report (nhtsa recall 15v-449), Jul. 15 2015.